Biointerface Research in Applied Chemistry
Open-Access Journal (ISSN: 2069-5837)

Article
Volume 16, Issue 4, 2026, 103
https://doi.org/10.33263/BRIAC164.103

LC-MS/MS Profiling and In Silico-Predicted Cyclooxygenase-2 (COX-2) Inhibitory Potential of Compounds from Togaku Rheumatic Oil

Erwince Fallo [1], Patrisius Maryanto Bria [1], Dimas Andrianto [1], R. Haryo Bimo Setiarto [2,3,*]

[1] Department of Biochemistry, Faculty of Mathematics and Natural Sciences, IPB University, Jl. Bungur No.1, Babakan, Dramaga, Bogor, West Java, 16680, Indonesia; 12345erlorlerwince@apps.ipb.ac.id (E.F.); patrisbria@apps.ipb.ac.id (P.M.B.); dimasandrianto@apps.ipb.ac.id (D.A.);
[2] Research Center for Applied Microbiology, National Research and Innovation Agency (BRIN), Jalan Raya Jakarta-Bogor Km 46, KST Soekarno, Cibinong, Bogor, West Java 16911, Indonesia; rhar002@brin.go.id;
[3] Research Collaboration Center for Traditional Fermentation, National Research and Innovation Agency (BRIN), Jl. Ir. Sutami 36 Kentingan, Jebres, Surakarta, Jawa Tengah, 57126, Indonesia; rhar002@brin.go.id;
* Correspondence: rhar002@brin.go.id;

Received: 30.04.2026; Accepted: 28.05.2026; Published: 15.08.2026

Abstract: This study investigated the chemical composition of Togaku rheumatic oil and computationally evaluated its cyclooxygenase-2 (COX-2)-related anti-inflammatory potential using an integrated LC–MS/MS, molecular docking, and in silico ADMET approach. LC–MS/MS profiling identified 13 putatively identified compounds, indicating a chemically complex multiherbal formulation. However, compound identification was based on database matching without confirmation using authentic standards, and relative peak areas were interpreted as semi-quantitative estimates rather than absolute concentrations. Among the detected compounds, Solanapyrone G was identified as the predominant annotated constituent. Molecular docking analysis revealed that Solanapyrone G and 6-undecylsalicylic acid exhibited favorable predicted binding interactions with the COX-2 active site, with docking scores (-9.922 kcal/mol) comparable to the reference ligand rofecoxib and higher than those of ibuprofen under the applied computational conditions. Solanapyrone G exhibited predicted interactions with key residues in the COX-2 active site, including ARG120, TYR355, and SER530, suggesting a plausible binding mode within the COX-2 active pocket. In contrast, 6-undecylsalicylic acid appeared to be stabilized predominantly through hydrophobic interactions within the binding pocket, with no distinct hydrogen-bond or electrostatic interactions detected in the 2D interaction analysis. Nevertheless, these computational results do not establish direct inhibitory potency, as no experimental COX-2 inhibition assay was performed in this study. Computational ADMET predictions further suggested that Solanapyrone G possesses a favorable pharmacokinetic and toxicity profile, characterized by good distribution, low predicted toxicity, and minimal risk of drug–drug interactions, although moderate intestinal absorption was predicted. Overall, these findings provide a preliminary chemical and computational basis supporting the traditional anti-inflammatory use of Togaku rheumatic oil while highlighting the need for further compound confirmation and experimental validation through in vitro and in vivo studies to substantiate its biological activity and safety.

Keywords: Togaku rheumatic oil; LC-MS/MS; molecular docking; COX-2; anti-inflammatory.

1. Introduction

Medicinal plants play an important role in public health and primary healthcare, particularly in developing countries, where plant-based remedies are widely used because they are accessible and culturally accepted as treatments [1-4]. In Indonesia, traditional medicine is still widely used, particularly in rural communities where access to modern healthcare may be limited [5]. A large household survey conducted in 2013 revealed that 30.4% of households utilized traditional healthcare [6]. In 2012, more than 280,000 traditional or alternative medicine practitioners were registered with the Indonesian Ministry of Health [7]. The majority (96.2%) used traditional healthcare methods, while 3.8% chose complementary healthcare methods such as acupuncture [5].

East Nusa Tenggara, Indonesia, is rich in medicinal plants traditionally used by local communities, particularly in South Central Timor (TTS) Regency [8]. Several plants commonly used in traditional medicine include *Carica papaya* L., *Acorus calamus* L., *Zingiber officinale* Roscoe, *Datura metel* L., *Justicia gendarussa* Burm.f., *Allium cepa* L., *Allium sativum* L., *Lantana camara* L., and *Cymbopogon citratus* (DC.) Stapf [8,9]. The people of Timor Island traditionally use both single- and mixed-plant medicinal preparations for healthcare. One traditional herbal product prepared by the people of Timor Island and used as a remedy for wounds, aches, and rheumatism is known as Togaku rheumatic oil.

Togaku rheumatic oil is traditionally prepared from a mixture of papaya roots (*Carica papaya* L.), genoak (*Acorus calamus* L.), ginger (*Zingiber officinale* Roscoe), datura leaves (*Datura metel* L.), gandarusa leaves (*Justicia gendarussa* Burm.f.), shallots (*Allium cepa* L.), garlic (*Allium sativum* L.), *Lantana camara* L. root, white damar bark (*Agathis dammara*), and lemongrass (*Cymbopogon citratus* (DC.) Stapf.), using coconut oil and gandapura oil as the base. Previous studies have reported that these plants contain various bioactive compounds, including saponins, flavonoids, phenolic compounds, and tannins identified in papaya and ganoak roots [10,11]. Ginger contains gingerols, shogaols, paradols, and zingerone [12]. Datura contains herpetol B [13], while gandarusa contains various bioactive compounds, including alkaloids, fatty acids, steroids, carotenoids, terpenoids, and the glycoside apigenin [14,15]. Garlic contains phenolic acids, especially gallic acid, ferulic acid, p-hydroxybenzoic acid, and chlorogenic acid [16]. Shallots contain organosulfur compounds and anthocyanins [17]; *Lantana camara* contains the binary compounds diodantunone and isodiodantunone [18], while lemongrass contains essential oil components such as citral, myrcene, farnesol, β-myrcene, and β-pinene [4,19]. These compounds may support the traditional use of Togaku rheumatic oil for wounds, aches, and rheumatic pain, as these conditions are associated with inflammatory processes, including COX-2-mediated prostaglandin production and pain.

Although there is literature on the chemical composition of the medicinal plants used to produce Togaku rheumatic oil, the product itself has never been analyzed for its chemical composition. COX-2 was selected as an initial molecular target because it plays a central role in prostaglandin biosynthesis, which contributes to inflammatory pain and swelling [20]. However, rheumatic pain and wound healing also involve other pathways, including COX-1 [21], lipoxygenases [22], pro-inflammatory cytokines, nitric oxide, oxidative stress, and NF-κB-related signaling [23]. Therefore, COX-2 docking in this study should be interpreted as an initial mechanistic prediction rather than a complete representation of the anti-inflammatory pathway. Therefore, this study aimed to conduct preliminary phytochemical profiling and tentative compound identification of Togaku rheumatic oil using LC-MS/MS, followed by

molecular docking analysis to predict the anti-inflammatory potential of the detected compounds against COX-2. In addition, in silico toxicity prediction was performed to provide preliminary safety information regarding the identified compounds. To the best of our knowledge, this is the first study to perform LC–MS/MS-based chemical profiling of Togaku rheumatic oil combined with molecular docking analysis against COX-2 and computational toxicity prediction. This study provides preliminary scientific evidence supporting the traditional use of Togaku rheumatic oil and may serve as a basis for future pharmacological and standardization studies.

2. Materials and Methods

2.1. Sample source.

The sample used in this study was a single commercially produced batch of Togaku rheumatic oil obtained from the Sinar Puinlam Kaenka Farmers Group in Tune Village, Tobu District, South Central Timor Regency, East Nusa Tenggara Province, Indonesia. The sample was analyzed directly without further processing. According to the producer, Togaku rheumatic oil is traditionally prepared by boiling a mixture of herbal ingredients, including papaya root (*Carica papaya* L.), genoak (*Acorus calamus* L.), ginger (*Zingiber officinale* Roscoe), datura leaves (*Datura metel* L.), gandarusa leaves (*Justicia gendarussa* Burm.f.), shallots (*Allium cepa* L.), garlic (*Allium sativum* L.), *Lantana camara* L. root, white damar bark (*Agathis dammara*), and lemongrass (*Cymbopogon citratus* (DC.) Stapf). The herbal ingredients were reportedly used in equal weight proportions (1:1, w/w). The herbal mixture was then boiled in coconut oil as the carrier oil, followed by the addition of gandapura oil during the final preparation step. Empirically, this product is used to help relieve bruising and swelling caused by impacts, treat postpartum wounds, and support wound healing through topical application. The oil is continuously manufactured using the same traditional formulation and preparation method. However, batch-to-batch variability was not evaluated in the present study because only a single production batch from a single producer was analyzed. Therefore, the resulting chemical profile should be considered preliminary and may not fully represent potential batch-to-batch or producer-to-producer variability.

2.2. Identification of active compounds.

Compounds in Togaku rheumatic oil samples were analyzed using an ultra-performance liquid chromatography–quadrupole time-of-flight mass spectrometry (UPLC-QTOF-MS) system (Xevo G2-S QTOF, Waters Corporation, Milford, MA, USA) at the National Police Forensic Laboratory Center, Sentul, Bogor, Indonesia. The analysis method was based on a previous method by Ismed *et al*. [24]. Before analysis, the oil sample was diluted in methanol to improve the solubility of detectable constituents within the oil matrix. The diluted sample was vortex-mixed, centrifuged to remove insoluble material, and filtered through a 0.2 µm membrane filter before LC–MS/MS injection. No additional lipid removal or fractionation procedure was performed. Compound separation was carried out using an ACQUITY UPLC BEH C18 column at 50°C with a gradient elution system. The mobile phase consisted of water containing 5 mM ammonium formate (phase A) and acetonitrile containing 0.05% formic acid (phase B), delivered at a flow rate of 0.2 mL/min, with a total analysis time of 23 min. A 5 µL sample volume was injected into the system.

Mass spectrometric detection was performed using electrospray ionization (ESI) in positive ion mode. The source temperature was maintained at 100 °C, and the desolvation temperature at 350 °C. The desolvation gas flow rate was set at 793 L/h, while the cone gas flow rate was maintained at 0 L/h. The mass range analysed was 50–1300 m/z, with low collision energy of 4 V and an elevated collision energy ramp of 25–70 V. Additional instrumental parameters, including capillary voltage, cone voltage, collision gas specification, scan rate, lock mass calibration, mass calibration procedure, and mass accuracy tolerance, were not available from the analytical facility documentation and therefore could not be retrospectively verified in the present study. The LC–MS/MS analysis was performed only in positive ionization mode because the method was primarily intended for preliminary screening of semi-polar and lipophilic constituents in the oil matrix. Consequently, certain acidic or highly polar metabolites that ionize preferentially in negative mode may not have been optimally detected.

Spectral data were processed using MassLynx software version 4.1. Compound annotation was performed primarily by comparing precursor ion masses and retention behavior against information available in the PubChem database (https://pubchem.ncbi.nlm.nih.gov/) and relevant literature. MS/MS fragmentation data were used as supporting evidence for tentative compound assignment when fragmentation information from published references was available. However, authentic reference standards, validated MS/MS spectral library matching, and retention time confirmation were not employed in the present study. Therefore, all reported compounds should be considered putative annotations corresponding approximately to MSI level 3 confidence according to accepted metabolomics reporting standards [25]. Methanol was used as the solvent blank during LC–MS/MS analysis. Nevertheless, detailed procedures for blank analysis, pooled quality-control samples, and replicate injections were not included in the analytical facility's documentation. They could not be confirmed retrospectively in the present study.

2.3. Enzyme structure selection and preparation.

Inhibition of the cyclooxygenase-2 (COX-2) enzyme is an approach in anti-inflammatory drug development, as it catalyzes the conversion of arachidonic acid into prostaglandins [26]. The three-dimensional (3D) structure of COX-2 was obtained from the Protein Data Bank (PDB) with accession code 5KIR (https://www.rcsb.org/structure/5KIR) [27]. This structure was chosen because it has a resolution of 2.70 Å, was determined by X-ray diffraction, and was crystallized with the selective inhibitor rofecoxib. The ligand rofecoxib was used as a reference ligand to define the binding site and serve as a control in molecular docking validation. Protein preparation was performed using YASARA Structure software. Although the original structure consists of chain A and chain B, only chain A was retained because it contains the catalytic binding pocket relevant for ligand interaction studies. Water molecules, ions (Mg, Ca, and Na), and the co-crystallized ligand were removed to minimize interference with docking calculations, and hydrogen atoms were added to optimize the protein structure. The prepared protein was then saved in PDB format. The removal of crystallographic water molecules and ions may alter local interactions within the native binding environment; therefore, docking results should be interpreted as a simplified computational representation of protein–ligand interactions. The quality of the protein structure was evaluated using the SAVES server, which includes ERRAT analysis [28], PROCHECK [29], PROVE [30], and Verify3D [31]. Next, structure validation was performed using the ProSA-web server [32]. In

the present study, only the PROCHECK and Verify3D results are presented and discussed in the main manuscript. In contrast, the ERRAT and ProSA-web validation results are provided in the Supplementary File.

2.4. Identification of the active protein pocket.

To confirm the suitability of the crystallographic binding region for docking analysis, active pocket prediction was additionally performed using the CavityPlus server version 2022.09 [33], despite the availability of the co-crystallized ligand rofecoxib in the 5KIR structure. The prepared protein structure was uploaded to the server, using chain A as the analysis target, and predictions were performed in the absence of a ligand with default parameters. The predicted major binding pocket corresponded to the binding region occupied by rofecoxib in the crystal structure, supporting the selection of this site for molecular docking. Therefore, the crystallographic ligand-binding site identified in the native rofecoxib complex was used as the primary docking region, with CavityPlus analysis as an additional validation step.

2.5. Ligand preparation.

The test ligands consisted of compounds putatively annotated from the LC–MS/MS profiling of Togaku rheumatic oil obtained from the Sinar Puinlam Kaenka Farmers Group, Tune Village, Tobu District, South Central Timor Regency, East Nusa Tenggara Province, Indonesia. SMILES data and the structures of each ligand were obtained from the PubChem database (https://pubchem.ncbi.nlm.nih.gov/) in *.sdf format. Ligand preparation was performed using YASARA Structure software. Hydrogen atoms were added using the “Clean All” function implemented in YASARA. The stereochemical configuration and tautomeric form of each ligand were assigned based on the structures available in the PubChem database, and no additional manual modification was performed. Partial atomic charges were assigned automatically by the YASARA force field during ligand preparation. Energy minimization was subsequently performed using the default YASARA minimization parameters to optimize the ligand geometry before docking analysis. Each prepared ligand was saved in *.pdb format. All prepared ligands were subsequently imported into YASARA and merged using the “Join” and “Transfer All Features” functions. The merged ligand file was then saved in *.sdf format as *_Ligands.sdf and used for molecular docking analysis [34].

2.6. Gridbox validation and molecular docking simulation.

Gridbox validation was performed using YASARA Structure software to verify the parameters used in the molecular docking process. Validation was conducted by redocking the reference ligand rofecoxib against the COX-2 protein using 999 redocking iterations [35]. The redocking results were evaluated based on the root-mean-square deviation (RMSD). An RMSD value below 2 Å was considered indicative of a valid docking protocol suitable for further molecular docking analysis. Molecular docking simulations were performed using YASARA Structure software following the method previously described by Gholam *et al.* [34]. The prepared ligand and COX-2 protein files were placed within a single working directory, and the YASARA dock_run macro (*.mcr) was used to execute the docking calculations. Before docking, the active site was defined based on the crystallographic binding region occupied by the co-crystallized ligand rofecoxib in the 5KIR structure, which was consistent with the major

cavity predicted by the CavityPlus analysis. Therefore, all docking simulations were focused on the native rofecoxib-binding pocket of chain A. The YASARA docking macro around the crystallographic rofecoxib-binding site automatically generated the docking search space. The grid box dimensions were set to 50 × 50 × 50 Å along the X, Y, and Z axes, respectively, with α, β, and γ angles fixed at 90°. Accordingly, docking simulations were spatially restricted to the native active pocket corresponding to the rofecoxib-binding region of the COX-2 structure.

All ligands were docked under identical docking conditions and simulation parameters. The docking protocol was configured to run 100 independent docking runs per ligand to improve conformational sampling and pose exploration. Hydrogen atoms were automatically added, and default YASARA force-field parameters were used throughout the docking procedure. Docked poses were clustered automatically using the default YASARA clustering algorithm. The representative binding pose for each ligand was selected as the pose with the highest docking score within the dominant docking cluster. Docking results were compared based on the YASARA scoring function scores. In the YASARA scoring convention used in this study, higher positive docking scores indicate relatively stronger predicted ligand–protein interactions within the software's internal scoring framework and were therefore used for comparative ligand ranking [34]. However, these values do not represent direct thermodynamic binding free energies. In molecular docking, more negative binding free energy values are typically associated with stronger, more favorable ligand–protein interactions. Therefore, the positive docking scores generated by YASARA in the present study should be interpreted only as relative comparative scores within the YASARA scoring system rather than as absolute thermodynamic binding affinity values.

2.7. ADMET prediction.

ADMET (absorption, distribution, metabolism, excretion, and toxicity) prediction was performed using the pkCSM online prediction platform (https://biosig.lab.uq.edu.au/pkcsm/prediction) [36], accessed on 24 April 2026. The analysis aimed to evaluate the predicted pharmacokinetic and toxicity profiles of selected compounds identified by LC–MS/MS profiling and molecular docking. SMILES representations of the ligands were retrieved from the PubChem database and used as input for the pkCSM prediction platform. ADMET prediction was performed for both Solanapyrone G and 6-undecylsalicylic acid because these compounds exhibited the highest docking scores in the molecular docking analysis of the COX-2 active site compared with ibuprofen, which was used as the positive control and a commercially available anti-inflammatory drug.

3. Results and Discussion

3.1. Profiling and identification of active compounds from Togaku rheumatic oil by LC-MS.

Togaku rheumatic oil, obtained from the Sinar Puinlam Kaenka Farmers Group, Tune Village, Tobu District, South Central Timor Regency, East Nusa Tenggara Province, Indonesia, was analyzed by LC–MS/MS to profile and putatively annotate the chemical constituents in the formulation. The resulting LC–MS chromatogram is presented in Figure 1, while details of the putatively annotated compounds are summarised in Table 1.

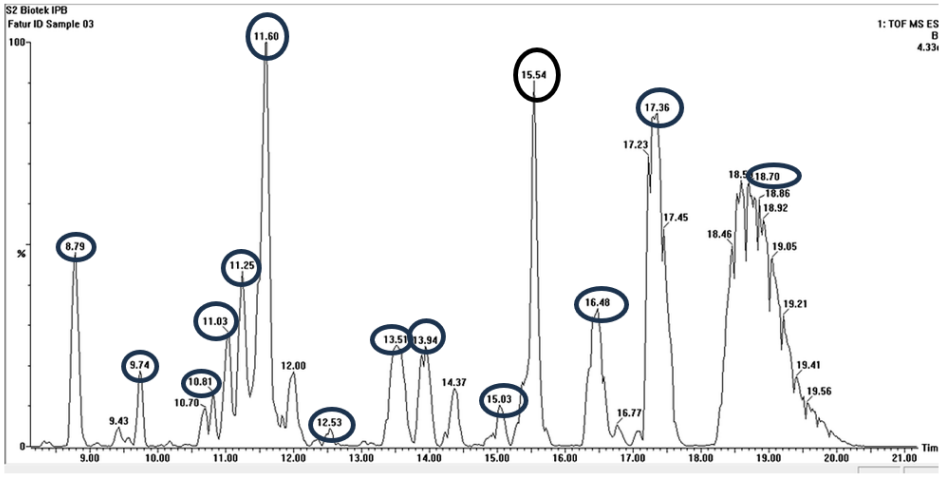

Figure 1. LC-MS chromatogram of Togaku rheumatic oil analysis results.

Table 1. Putatively annotated compounds detected by LC-MS analysis of Togaku rheumatic oil.

RT (min)	Name of compound	PubChem CID	Molecular formula	Exact mass (Da)	Peak area (%)	Observed m/z	Theoretical m/z	Mass error (ppm)
8.79	2,6-Dimethoxy-1-acetonylquinol	241783	$C_{11}H_{14}O_5$	226.0841	5.88	227.09	227.0914	-6.16
9.74	Sesamin dicatechol	46881231	$C_{18}H_{18}O_6$	330.1103	2.56	331.12	331.1176	7.25
10.82	(3β,22E)-Chola-5,22-dien-3-ol	21159718	$C_{24}H_{38}O$	342.2923	3.76	343.30	343.2996	1.17
11.03	Rubiginosin B	11269635	$C_{21}H_{22}O_8$	402.1315	5.85	403.14	403.1388	2.98
11.25	5,7,3',4'-Tetramethoxyflavone	631170	$C_{19}H_{18}O_6$	342.1103	9.93	343.12	343.1176	6.99
11.58	Solanapyrone G	10755717	$C_{17}H_{21}NO_3$	287.1521	19.61	288.16	288.1594	2.08
12.53	6-Undecylsalicylic acid	10946274	$C_{18}H_{28}O_3$	292.2038	1.08	293.21	293.2111	-3.75
13.51	3,5-Diphenylpyrazole	70840	$C_{15}H_{12}N_2$	220.1000	7.11	221.11	221.1073	12.21
14.37	Linolenic acid	5280934	$C_{18}H_{30}O_2$	278.2246	3.70	279.23	279.2319	-6.81
15.54	7-[[4-(1-Phenylethoxy)phenyl]methyl]-7-propan-2-ylbicyclo[2.2.1]hepta-1,3,5-triene	91431623	$C_{25}H_{25}O$	341.1905	13.86	342.20	342.1978	6.43
16.48	Oxalic acid, 1-menthyl nonyl ester	6421330	$C_{21}H_{38}O_4$	354.2770	5.03	355.29	355.2843	16.04
17.36	4,4'-(Methylenedicyclohexane-1,4-diyl)bis(1,1-dimethylsemicarbazide)	12035238	$C_{19}H_{38}N_6O_2$	382.3056	11.67	383.31	383.3129	-7.57
18.70	N-[4-(dodecylamino)-6-[hydroxy(propyl)amino]-1,3,5-triazin-2-yl]-N-propylhydroxylamine	134935968	$C_{21}H_{42}N_6O_2$	410.3369	9.97	411.34	411.3442	-10.21

RT = retention time; CID = PubChem Compound Identification Number; Peak Area (%) indicates relative peak area abundance. All ions were detected in positive ionization mode as protonated molecular ions ([M+H]+). Compound annotation was tentatively assigned based on observed m/z values and comparison with the PubChem database.

LC-MS identification revealed that Togaku rheumatic oil contains 13 putatively annotated compounds, as shown in Table 1. This profile reflects a complex chemical composition, in line with the characteristics of Togaku rheumatic oil, a multiherbal formulation composed of various natural ingredients such as papaya root (*Carica papaya* L.), genoak (*Acorus calamus* L.), ginger (*Zingiber officinale* Roscoe), datura leaves (*Datura metel* L.), gandarusa leaves (*Justicia gendarussa* Burm.f.), shallots (*Allium cepa* L.), garlic (*Allium sativum* L.), *Lantana camara* L. root, white damar bark (*Agathis dammara*), and lemongrass (*Cymbopogon citratus* (DC.) Stapf.), coconut oil, and gandapura oil. These compounds were detected at retention times (RTs) of 8.79–18.70 minutes, with a total relative area of

approximately 100.01%, indicating that the putatively annotated compounds accounted for most of the detected chromatographic peak area. However, unidentified low-abundance compounds, co-eluting features, and ionization-related limitations may still be present. Solanapyrone G showed the highest relative MS peak response (19.61%), followed by 7-[[4-(1-phenylethoxy)phenyl]methyl]-7-propan-2-ylbicyclo[2.2.1]hepta-1,3,5-triene (RT 15.54 min; 13.86%), 4,4'-(Methylenedicyclohexane-1,4-diyl)bis(1,1-dimethylsemicarbazide) (11.67%), N-[4-(dodecylamino)-6-[hydroxy(propyl)amino]-1,3,5-triazin-2-yl]-N-propylhydroxylamine (RT 18.70 min; 9.97%), and 5,7,3',4'-tetramethoxyflavone (9.93%). The LC-MS chromatogram (Figure 1) showed the highest-intensity peak at RT around 11.58 minutes, followed by a dominant cluster of peaks at RT 15.54, 17.36, and 18.70 minutes. This pattern suggests that many detected constituents were enriched in the middle- to late-elution fractions, which are generally associated with semi-polar to lipophilic compounds.

It should be noted that relative peak areas in LC–MS analysis reflect signal intensity within a single analytical run and do not directly reflect absolute compound concentrations. Mass spectrometric responses are strongly influenced by ionization efficiency, matrix effects, and physicochemical properties of individual compounds, such that compounds at similar concentrations may produce different signal intensities [37]. Therefore, the quantitative interpretation of the present data should be considered semi-quantitative and exploratory. Several putatively annotated compounds detected in Togaku rheumatic oil belong to chemical classes previously reported to possess antioxidant and anti-inflammatory activities. For example, 5,7,3',4'-tetramethoxyflavone is a polymethoxyflavone derivative that has previously been associated with antioxidant and anti-inflammatory properties. This compound may potentially originate from herbal ingredients such as shallots and gandarusa. In addition, compounds such as linolenic acid, sesamin dicatechol, and 6-undecylsalicylic acid have been reported to exhibit anti-inflammatory potential by modulating inflammatory mediators and cellular signaling pathways.

Interestingly, several characteristic compounds commonly reported in the individual herbal ingredients, such as gingerols and shogaols from ginger, organosulfur compounds from garlic and shallots, and volatile constituents such as citral from lemongrass, were not prominently detected in the LC–MS profile. This observation may be associated with several analytical and processing-related factors. LC–MS operated under conventional reversed-phase conditions is generally more suitable for semi-polar and non-volatile compounds, whereas highly volatile constituents are more effectively analyzed by GC–MS. In addition, thermal processing during the preparation of Togaku rheumatic oil may contribute to degradation, volatilization, oxidation, or chemical transformation of thermolabile compounds. For example, gingerols may undergo thermal conversion to shogaols, while volatile organosulfur compounds may oxidize or evaporate during heating [38,39].

The use of coconut oil as the extraction medium may also influence the detected phytochemical profile. Lipid-based solvents generally favor the extraction of lipophilic constituents, whereas highly polar or ionic compounds may be extracted less efficiently. In addition, the complex matrix of multiherbal oil formulations may produce matrix effects, such as ion suppression or enhancement, during mass spectrometric analysis [40]. These phenomena can alter signal intensities and potentially mask compounds with lower ionization efficiency or lower abundance. Consequently, some constituents originating from the herbal ingredients may not have been optimally detected under the analytical conditions used in the present study.

The LC–MS/MS profiling of Togaku rheumatic oil highlights the chemical complexity typical of multiherbal lipid-based formulations, in which diverse phytochemicals from different botanical sources coexist within a single extract. The detection of 13 putatively annotated metabolites within a relatively narrow retention time window (8.79–18.70 min) suggests a selective enrichment of semi-polar to lipophilic constituents, which is consistent with the use of coconut oil as the extraction medium. This solvent system likely favors the partitioning of hydrophobic bioactive molecules, thereby shaping the observed metabolite profile toward compounds with moderate to low polarity. The predominance of compounds such as Solanapyrone G and several structurally complex derivatives may reflect genuine phytochemical constituents or tentative annotations due to limitations in database matching. In untargeted LC–MS workflows, compound identification at this level generally corresponds to putative annotation (Level 3 confidence), where spectral similarity does not necessarily confirm structural identity. This is particularly relevant for complex herbal matrices, where isomeric or structurally related compounds may yield similar fragmentation patterns. Therefore, confirmatory analysis using authentic standards or complementary techniques, such as NMR, would be required to validate the identities of the major compounds detected.

Several putatively detected constituents in Togaku rheumatic oil belong to chemical classes previously associated with anti-inflammatory activity, including polymethoxyflavones, fatty acids, and phenolic derivatives. Compounds belonging to these classes have been reported to modulate inflammatory pathways through mechanisms such as cyclooxygenase inhibition, suppression of pro-inflammatory cytokines, and regulation of oxidative stress responses. Therefore, the detected phytochemical profile may partially support the ethnopharmacological use of Togaku rheumatic oil for inflammatory-related conditions. The coexistence of multiple compounds with potentially overlapping mechanisms may also suggest synergistic interactions, as commonly proposed in traditional herbal formulations. However, because several compound annotations remain tentative and biological evidence for some detected constituents is still limited, further experimental validation is necessary to confirm their pharmacological relevance and biological activity.

From a pharmacological perspective, several compounds identified in Togaku rheumatic oil belong to chemical classes previously associated with anti-inflammatory activity, suggesting potential multi-target mechanisms involving multiple inflammatory pathways. However, because several compound annotations remain tentative and the present LC–MS/MS analysis was semi-quantitative, additional studies involving compound isolation, structural confirmation, quantitative analysis, and biological validation are required to clarify the contribution of individual constituents and their potential synergistic interactions. Overall, this study provides a preliminary chemical fingerprint of Togaku rheumatic oil and lays the foundation for future standardization, quality control development, and pharmacological investigation. Integration of complementary analytical platforms such as GC–MS and NMR, together with bioassay-guided fractionation, would further strengthen compound identification and biological interpretation.

3.2. Enzyme selection and preparation.

The cyclooxygenase-2 (COX-2) enzyme was selected as the molecular target because of its established role in inflammatory processes, including prostaglandin-mediated pain and swelling [41]. Analysis of the protein structure was performed by removing crystallographic water molecules, ions (Na, Mg, and Ca), and other non-essential molecules, followed by adding

hydrogen atoms to optimize the docking environment [34]. Structure validation of the COX-2 protein structure using PROCHECK (Figure 2A) showed that most residues were located within acceptable regions of the Ramachandran plot, with 88.3% in the most favored region and only 0.1% in the disallowed region. Although the percentage of residues in the most favored region was slightly below the commonly recommended threshold, the very low proportion of disallowed residues indicates that the overall stereochemical quality of the protein structure remained acceptable for molecular docking analysis.

Verify3D analysis (Figure 2B) showed that 76.36% of residues had an average 3D–1D score ≥ 0.1, slightly below the commonly recommended 80% threshold. This suggests that certain regions of the protein may exhibit reduced structural compatibility, potentially due to flexible loops or local conformational variability. However, these deviations were not predominantly located within the rofecoxib-binding pocket used for docking simulations. In molecular docking studies, the structural reliability of the active-site region is generally considered more critical than minor deviations in peripheral or flexible regions of the protein structure. Therefore, the active-site region of the COX-2 structure was considered sufficiently reliable for ligand docking and interaction studies.

Visualization of residue distribution by Ramachandran categories (Figure 2C) further showed that most residues were located in the most favored regions. In contrast, only a very small number of residues were positioned in generously allowed or disallowed regions. Importantly, these residues were not concentrated around the active-site region used for docking analysis. Collectively, these results indicate that the COX-2 structure possesses acceptable global and active-site structural reliability for the molecular docking study performed in the present work.

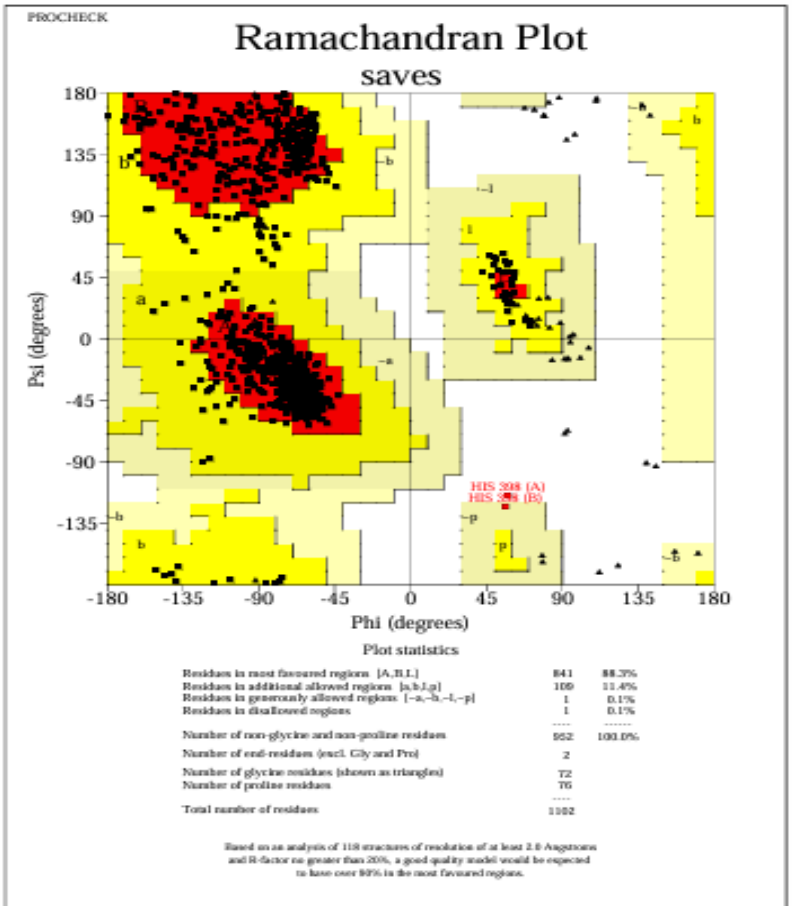

(a)

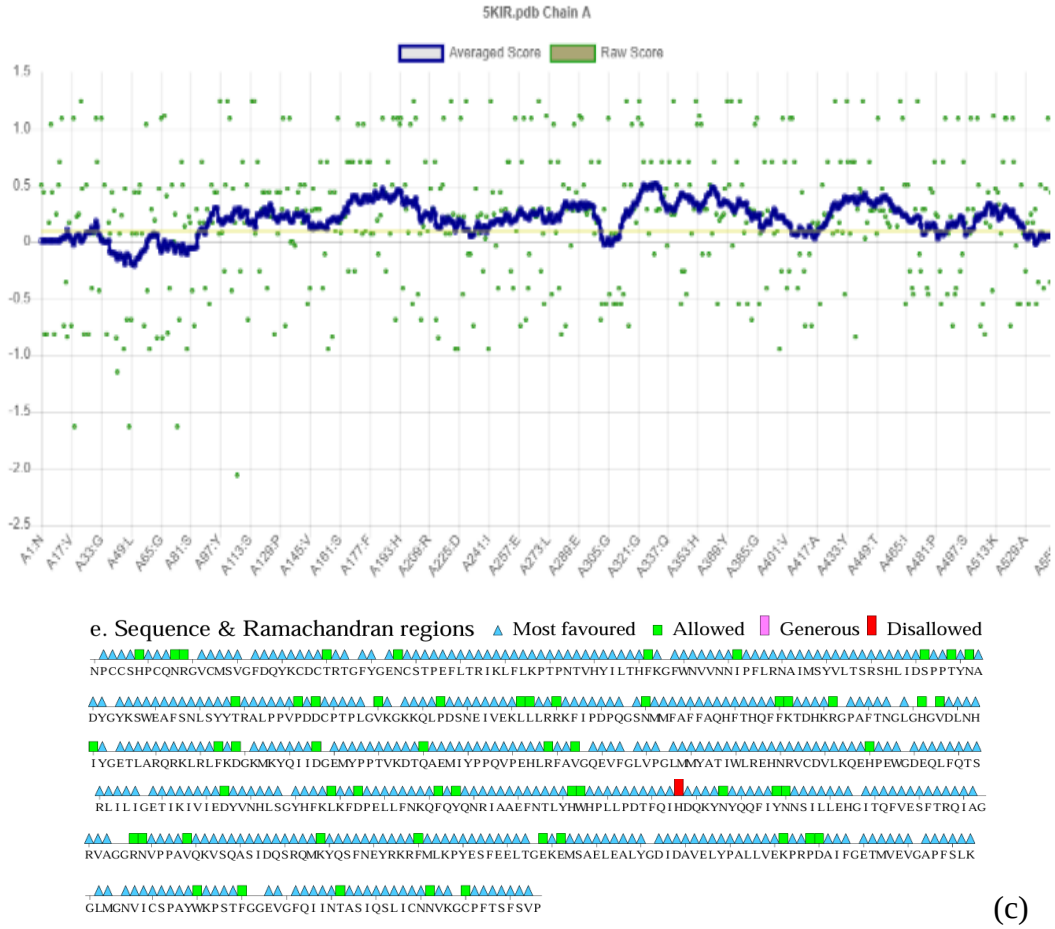

Figure 2. Validation of the COX-2 protein structure using **(a)** PROCHECK Ramachandran plot analysis; **(b)** Verify3D analysis; **(c)** and visualization of residue distribution based on Ramachandran categories along the protein sequence. Additional validation results from ProSA-web and ERRAT analyses are provided in the supplementary material.

3.3. Identification of the active protein pocket.

The active protein pocket is a critical component that requires analysis to ensure the ligand-binding site on the target protein is located at a site that inhibits the protein's biological activity [42]. Binding pocket identification was performed using the CavityPlus web server, which generated several candidate binding pockets for the COX-2 protein. The pocket selection was based on several parameters, namely druggability, a high DrugScore, and adequate pocket size, as indicated by surface area and volume. Furthermore, high Pred Max and Pred Ave pKd values were considered when determining the best pocket. The prediction results revealed 15 binding pockets, each with its own parameters, as presented in Table 2.

Table 2. Results of the prediction of binding pockets in the COX-2 protein using cavityPlus.

No. Cavity	Pred Max pKd	Pred Ave pKd	DrugScore	Druggability
1	10.99	6.97	-704.00	Undruggable
2	11.05	6.97	4217.00	Druggable
3	11.65	6.87	2960.00	Druggable
4	11.79	6.80	4.00	Less druggable
5	11.76	6.65	3795.00	Druggable
6	10.87	6.34	-1036.00	Undruggable
7	10.82	6.33	1157.00	Druggable
8	9.17	5.76	-1254.00	Undruggable
9	8.63	5.58	-1085.00	Undruggable
10	7.78	5.29	-756.00	Undruggable
11	7.75	5.27	-1060.00	Undruggable

No. Cavity	Pred Max pKd	Pred Ave pKd	DrugScore	Druggability
12	7.47	5.18	-901.00	Undruggable
13	6.85	4.97	-980.00	Undruggable
14	6.81	4.95	-879.00	Undruggable
15	6.31	4.78	-1177.00	Undruggable

Pred Max pKd and Pred Ave pKd indicate predicted binding affinities. DrugScore represents pocket feasibility, while druggability indicates the predicted ability of the pocket to bind small ligands.

Based on the obtained parameters, cavity number 2 was selected as the primary active site because it had the highest DrugScore (4217.00) and was categorized as druggable. Several other cavities were also classified as druggable, but had lower DrugScore values than cavity 2. Meanwhile, cavity 1, despite its relatively large size, was not selected because it was undruggable and had a negative DrugScore (-704.00), indicating that the pocket did not support optimal ligand interaction. According to Sun *et al*. [43], undruggable targets are proteins that have therapeutic significance but are difficult to target using conventional drug design approaches. This can be due to unique characteristics such as a highly dynamic structure, the lack of a well-defined ligand-binding pocket, or a highly conserved active site.

Analysis of the residues composing cavity 2 (Table 3) revealed the presence of several key residues associated with the active site of the COX-2 enzyme, including ARG120, TYR355, SER530, VAL523, ARG513, GLY526, ILE517, PHE518, VAL349, and LEU352. Comparison with the interaction profile of the co-crystallized ligand rofecoxib (Table 4) showed substantial overlap between the predicted cavity residues and the crystallographic binding site. Notably, approximately 17 major residues involved in rofecoxib binding, including HIS90, ARG120, GLN192, TYR348, VAL349, LEU352, SER353, TYR355, ARG513, ILE517, PHE518, MET522, VAL523, GLY526, ALA527, SER530, and LEU531, were also identified within cavity 2, supporting that this cavity corresponds to the biologically relevant active pocket of COX-2. These residues are known to contribute to ligand recognition and stabilization within the COX-2 binding site [44-46]. Therefore, cavity 2 was selected as the docking site to ensure that ligand–protein interactions were analyzed within a biologically relevant binding region.

Table 3. Characteristics of selected binding pockets (Cavity 2) and their constituent residues based on cavityplus analysis.

No	Surface area (Å2)	Volume (Å3)	Box Size (Å)	Box Center (Å)	Residues
2	1478.50	2422.62	23.0 27.0 17.5	14.0 7.0 28.75	SER-119, VAL-525, PHE-81, MET-471, HIS-122, LEU-93, ILE-345, GLU-73, LEU-82, PRO-72, LEU-117, THR-62, LEU-108, SER-126, VAL-523, SER-353, ARG-513, MET-522, LYS-369, GLY-526, ILE-112, LEU-80, VAL-89, THR-85, THR-76, THR-88, GLN-192, VAL-349, TYR-91, GLY-354, LEU-359, THR-60, LEU-384, ILE-517, LEU-531, LYS-473, SER-530, PHE-529, PHE-381, GLY-45, GLN-42, LYS-468, LYS-83, THR-118, VAL-103, ALA-111, ARG-120, VAL-116, GLU-524, ARG-469, THR-94, SER-114, ASN-43, ARG-467, LEU-75, LEU-123, ASN-350, LEU-352, PHE-99, TYR-348, PRO-528, HIS-351, LYS-79, ARG-44, LEU-472, SER-70, CYS-69, PRO-86, SER-121, ASP-125, ILE-78, ALA-527, PHE-357, PRO-84, PHE-371, ILE-92, PHE-64, ASN-87, PHE-470, ARG-61, ARG-77, TYR-115, ILE-124, GLN-370, GLY-63, TRP-100, TYR-355, HIS-90, PHE-518, MET-113

Surface area (Å²) and volume (Å³) describe the binding pocket size. Box size and box center (Å) indicate the docking grid parameters. Residues in cavity 2 represent amino acids involved in ligand–protein interactions.

To validate the predicted binding site, overlay visualization of rofecoxib, binding cavity 2, and the COX-2 protein structure was performed using PyMOL. This analysis was conducted to evaluate the spatial correspondence between the selected cavity and the native ligand-binding site. The results are presented in Figure 3. The overlay visualization from different orientations revealed the spatial relationships among rofecoxib, binding cavity 2, and the COX-2 protein structure. Panel A shows the front view, Panel B presents the side view following a 90° rotation, and Panel C illustrates the internal pocket view. Rofecoxib was located within the active-site region of the COX-2 protein, while binding cavity 2 spatially overlapped with the ligand-binding region. The close alignment between rofecoxib and cavity 2 demonstrates that the selected cavity corresponds to the enzyme's biologically relevant active-site region. These findings support the suitability of cavity 2 as the docking site for evaluating interactions between compounds from Togaku rheumatic oil and the COX-2 protein.

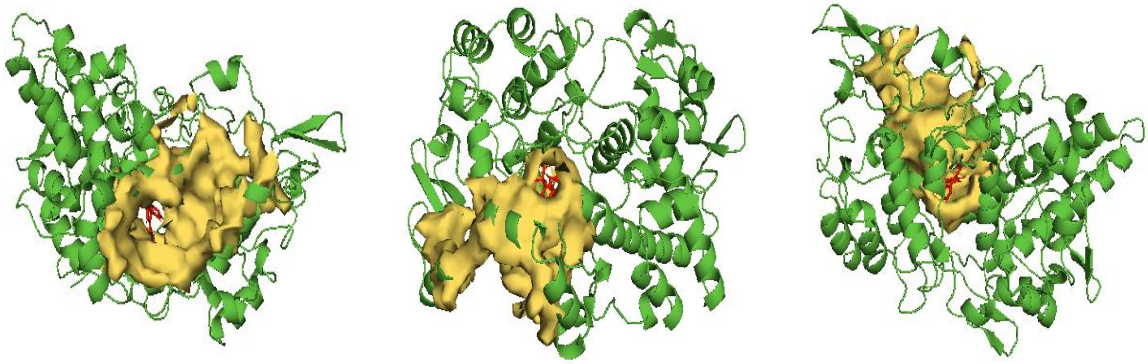

(a) **(b)** **(c)**

Figure 3. Overlay visualization of rofecoxib (red stick), binding cavity 2 (yellow surface), and the COX-2 protein structure (green cartoon) generated using PyMOL. The figure is shown from different orientations: **(a)** front view; **(b)**side view (90° rotation); **(c)** inside pocket view.

3.4. Ligand preparation.

Ligand preparation optimizes ligand structure for molecular docking simulations. This process involves adding hydrogen atoms to complete the molecular structure, enabling interactions such as hydrogen bonds to be properly identified. Furthermore, energy minimization is performed to obtain an energetically stable ligand conformation, thereby increasing the accuracy of the docking results [47].

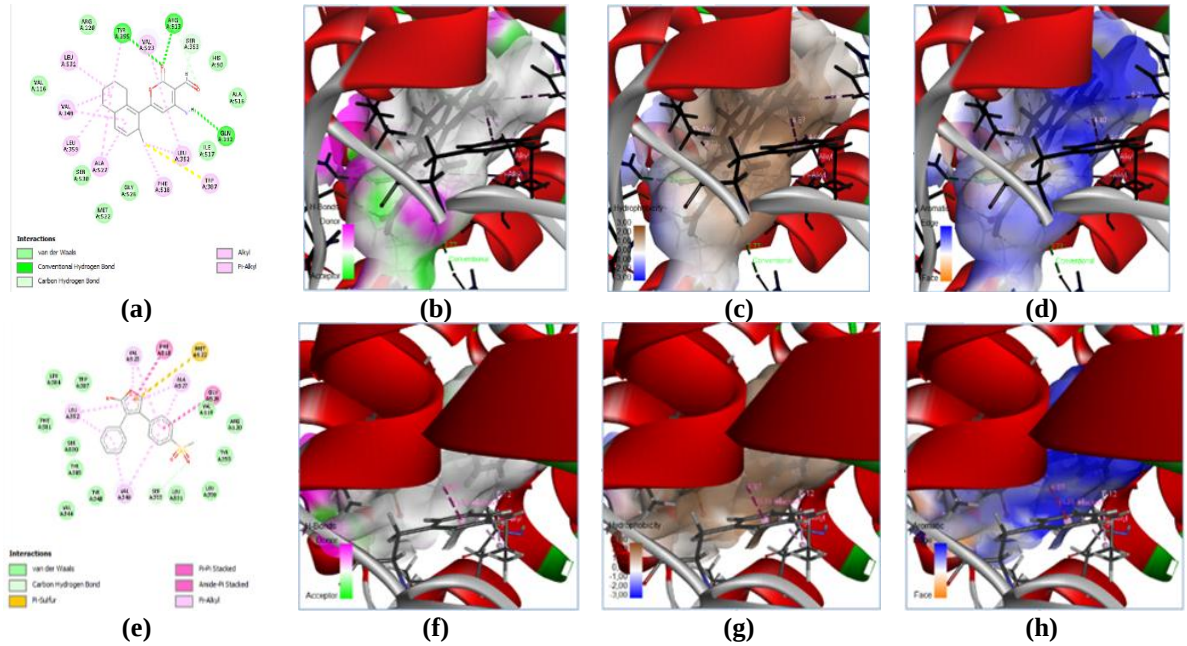

(a) **(b)** **(c)** **(d)**

(e) **(f)** **(g)** **(h)**

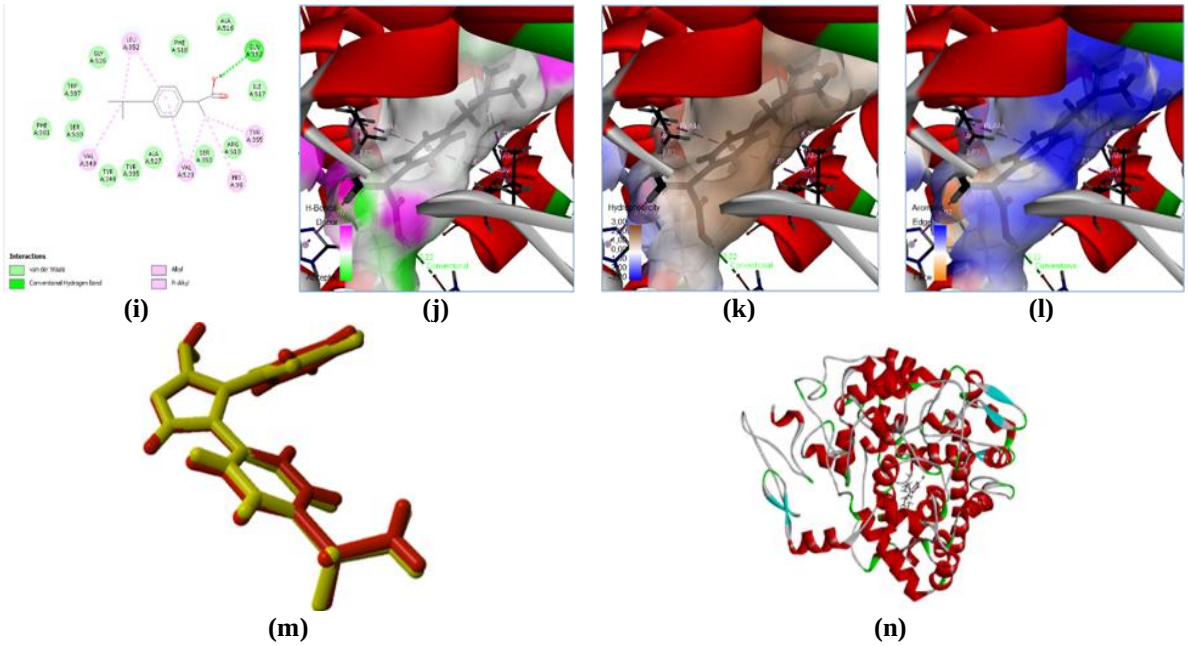

Figure 4. Visualization of ligand–protein interactions within the active pocket of the COX-2 enzyme generated using Discovery Studio Visualizer. Panels **(a–d)** represent the interaction profile of Solanapyrone G, including the 2D interaction diagram, 3D hydrogen-bond interactions, hydrophobic interactions, and aromatic interactions, respectively. Panels **(e–h)** show the interaction profile of the native ligand rofecoxib, while panels (i–**l)** illustrate the interaction profile of the positive control ibuprofen with the same interaction sequence. Panel **(m)** shows ligand validation by redocking, demonstrating the conformity of the docked ligand orientation with the native ligand in the protein active site, whereas panel **(n)** presents the 3D interaction of 6-undecylsalicylic acid within the active pocket of the COX-2 enzyme. All interaction visualizations include residue labels, interaction types, and bond-distance annotations.

3.5. Gridbox validation and molecular docking simulation.

Gridbox validation is performed by redocking the reference ligand rofecoxib against the COX-2 enzyme. The parameter used to evaluate validation success is the Root Mean Square Deviation (RMSD), which measures the agreement between the docked ligand position and the reference structure and allows analysis of differences in ligand conformation and orientation [48]. In general, an RMSD < 2 Å is considered a good indicator of a docking protocol's validation [49]. The redocking results yielded an RMSD of 1.6131 Å, below the threshold. This value indicates that the docking parameters used accurately reproduced the native ligand position in the enzyme's active site. Visualization of the ligand position before and after redocking (Figure 4) also demonstrated the conformity of the ligand orientation in the binding pocket. Thus, the docking protocol used was declared valid and can be applied to subsequent molecular docking simulations. The molecular docking simulation yielded a key parameter, the binding energy (kcal/mol), which describes the strength and stability of the ligand-receptor interaction. The binding energy values for each docked compound against the COX-2 enzyme are presented in Table 4.

Table 4. Molecular docking results of test compounds against the COX-2 enzyme.

Name of compound	Binding energy (kcal/mol)	Predicted ligand–COX-2 interaction residues			
		Hydrogen bond	Hydrophobic and van der Waals Interaction	π-interactions	Other interactions
Rofecoxib (Native ligand of COX-2)	9.927	HIS90, ARG120, GLN192, SER353, TYR355, ARG513, SER530	VAL349, LEU352, ALA516, ILE517, MET522, VAL523, ALA527, LEU531	TYR348, TYR355, TYR385, TRP387, PHE518	GLY526

Name of compound	Binding energy (kcal/mol)	Predicted ligand–COX-2 interaction residues			
		Hydrogen bond	Hydrophobic and van der Waals Interaction	π-interactions	Other interactions
Ibuprofen (positive control)	8.084	HIS90, GLN192, SER353, TYR355, ARG513, SER530	VAL349, LEU352, ALA516, ILE517, VAL523, ALA527	TYR348, TYR355, PHE381, TYR385, TRP387, PHE518	GLY526
Solanapyrone G	9.922	HIS90, ARG120, GLN192, SER353, TYR355, ARG513, SER530	VAL116, VAL349, LEU352, LEU359, ALA516, ILE517, VAL523, ALA527, LEU531	TYR355, TRP387, PHE518	GLY526
6-Undecylsalicylic acid	9.922	HIS90, ARG120, GLN192, SER353, TYR355, ARG513, SER530	VAL116, VAL349, LEU352, LEU359, ALA516, ILE517, VAL523, ALA527, LEU531	TYR355, TRP387, PHE518	GLY526
3,5-Diphenylpyrazole	8.684	HIS90, GLN192, SER353, TYR355, ARG513, SER530	VAL349, LEU352, LEU384, ALA516, ILE517, MET522, VAL523	TYR348, TYR355, PHE381, TYR385, TRP387, PHE518	GLY526
2,6-Dimethoxy-1-acetonylquinol	7.586	HIS90, ARG120, SER353, TYR355, SER530	VAL116, VAL349, LEU352, LEU359, ILE517, VAL523, ALA527, LEU531	TYR355, TRP387, PHE518	GLY526
Linolenic acid	7.289	HIS90, ARG120, GLN192, SER353, TYR355, ARG513, SER530	VAL116, VAL349, LEU352, LEU359, LEU384, ALA516, ILE517, MET522, VAL523, ALA527, LEU531	TYR348, TYR355, PHE381, TYR385, TRP387, PHE518	GLY526
5,7,3',4'-Tetramethoxyflavone	6.184	HIS90, ARG120, GLN192, SER353, TYR355, ARG513, SER530	VAL344, VAL349, LEU352, LEU384, ALA516, ILE517, MET522, VAL523, ALA527, LEU534	PHE205, TYR348, TYR355, PHE381, TYR385, TRP387, PHE518	GLY526
Oxalic acid, 1-menthyl nonyl ester	6.184	HIS90, ARG120, GLN192, SER353, TYR355, ARG513, SER530	VAL344, VAL349, LEU352, LEU384, ALA516, ILE517, MET522, VAL523, ALA527, LEU534	PHE205, TYR348, TYR355, PHE381, TYR385, TRP387, PHE518	GLY526
N-[4-(dodecylamino)-6-[hydroxy(propyl)amino]-1,3,5-triazine-2-yl]-N-propylhydroxylamine	5.962	HIS90, ARG120, GLN192, SER353, TYR355, ARG513, SER530	MET113, VAL116, VAL344, VAL349, LEU352, LEU359, LEU384, ALA516, ILE517, MET522, VAL523, ALA527, LEU531, LEU534	PHE205, TYR348, TYR355, PHE381, TYR385, TRP387, PHE518	
7-[[4-(1-Phenylethoxy)phenyl]methyl]-7-propan-2-ylbicyclo[2.2.1]hepta-1,3,5-triene	3.807	ARG120, SER353, TYR355, SER530	VAL116, VAL349, LEU352, LEU359, VAL523, ALA527, LEU531	TYR348, TYR355, PHE381, TYR385, TRP387, PHE518	GLY526
Sesamin dicatechol	3.198	HIS90, GLN192, SER353, TYR355, ARG513, SER530	VAL344, ILE345, VAL349, LEU352, ALA516, ILE517, MET522, VAL523, ALA527, LEU531, LEU534	PHE205, TYR348, TYR355, TYR385, TRP387, PHE518	GLY526
(3β,22E)-Cholesta-5,22-dien-3-ol	1.339	HIS90, ARG120, GLN192, SER353, TYR355, ARG513, SER530	VAL344, VAL349, LEU352, ALA516, ILE517, VAL523, ALA527, LEU531, LEU534	PHE205, TYR348, TYR355, TYR385,	GLY354, GLY526

Name of compound	Binding energy (kcal/mol)	Predicted ligand–COX-2 interaction residues			
		Hydrogen bond	Hydrophobic and van der Waals Interaction	π-interactions	Other interactions
				TRP387, PHE518	
Rubiginosin B	-2.133	HIS90, THR94, GLN192, SER353, TYR355, ASP515, GLU520, SER530	VAL344, VAL349, LEU352, LEU359, PRO514, ALA516, ILE517, VAL523, ALA527, LEU531, LEU534	PHE205, TYR348, TYR355, PHE381, TYR385, PHE518	
4,4′-(Methylenedicyclohexane-1,4-diyl)bis(1,1-dimethylsemicarbazide))	-27.215	HIS90, ARG120, GLN192, SER353, TYR355, ARG513, SER530, GLU524	LEU93, VAL116, VAL344, VAL349, LEU352, LEU359, PRO512, ALA516, ILE517, VAL523, ALA527, LEU531, LEU534	PHE205, TYR348, TYR355, PHE381, TYR385, PHE518	GLY519 ARG120, ARG513, GLU524

Hydrogen bonds, hydrophobic/van der Waals interactions, π interactions, and other interactions were predicted using molecular docking analysis in YASARA Structure. Hydrophobic and van der Waals interactions were grouped because YASARA Structure reports these contacts within the same interaction category.

Molecular docking simulations showed that all test compounds exhibited varying docking scores toward the COX-2 enzyme, ranging from −27.215 to 9.922 kcal/mol. In the YASARA Structure calculation system used in this study, higher positive score values correspond to relatively stronger predicted ligand–protein interactions within the docking framework and were used for comparative ligand ranking. Based on these results, Solanapyrone G and 6-undecylsalicylic acid exhibited the highest docking scores (9.922 kcal/mol), which were comparable to the selective COX-2 reference ligand rofecoxib (9.927 kcal/mol) and higher than that of ibuprofen (8.084 kcal/mol) under the applied computational conditions. However, ibuprofen was included only as a representative non-selective NSAID comparator; therefore, differences in docking scores should not be interpreted as direct evidence of relative COX-2 selectivity or inhibitory potency. Furthermore, these docking scores represent only relative computational predictions and do not directly correspond to experimental binding affinity, inhibitory activity, or pharmacological efficacy.

Further interaction analysis showed that Solanapyrone G exhibited interaction patterns involving key active-site residues, including ARG120, TYR355, and SER530, which are commonly associated with ligand recognition within the COX-2 binding pocket. In contrast, although 6-undecylsalicylic acid occupied the same binding region and showed a comparable docking score, its interaction profile was dominated by hydrophobic contacts, with no clearly defined specific interactions in the 2D interaction analysis. These findings suggest that both compounds may be accommodated within the biologically relevant active site of COX-2 under the computational conditions applied. Most ligand–protein complexes involved residues commonly associated with the COX-2 active site, including HIS90, ARG120, GLN192, TYR355, TRP387, ARG513, and SER530.

In addition, hydrophobic residues such as VAL349, LEU352, ILE517, PHE518, MET522, and VAL523 were frequently involved in ligand interactions, indicating the importance of hydrophobic contacts in stabilizing the predicted ligand–protein complexes [49,50]. Rofecoxib, as the co-crystallized reference ligand, exhibited a well-defined interaction profile involving hydrogen-bonding, hydrophobic, and π-interactions within the COX-2 active site. The similarity of several predicted interaction residues between the test compounds and rofecoxib suggests that these ligands may occupy a binding region similar to that of the reference ligand. Nevertheless, further experimental studies are required to confirm their actual COX-2 inhibitory activity and binding mechanisms. A visualization of the ligand-COX-2

complex, which has a binding energy value greater than that of the positive control, is shown in Figure 4.

Based on the 2D visualization, Solanapyrone G exhibited several important interactions with key COX-2 residues, including ARG120, SER530, and TYR355, which are known to contribute to ligand anchoring, hydrogen bonding, and stabilization within the active site. In addition, hydrophobic residues such as VAL349, LEU352, and PHE518 may enhance complex stability through hydrophobic and van der Waals interactions. These findings are consistent with the 3D visualization, which demonstrated that Solanapyrone G was well accommodated within the COX-2 active pocket and adopted a stable binding orientation. Such interactions may contribute to the favorable binding affinity observed in the docking analysis.

Ibuprofen, used as a positive control, exhibited a similar interaction pattern, although the interactions appeared less extensive than those observed for Solanapyrone G and rofecoxib. This was reflected by the reduced involvement of key active-site residues, particularly ARG120, which is recognized as an important residue in COX-2 inhibitor binding. The 3D visualization further indicated that ibuprofen occupied the active pocket in a less optimal orientation than ligands with higher binding affinity. Meanwhile, the native ligand rofecoxib showed the most comprehensive interaction profile, involving hydrogen bonds, hydrophobic interactions, and electrostatic interactions with several key residues. The 3D visualization confirmed that rofecoxib adopted a stable conformation that closely matched the geometry of the active pocket, thereby supporting its strong binding affinity toward COX-2.

Interestingly, the 2D visualization of 6-undecylsalicylic acid did not reveal specific interaction types such as hydrogen bonds or electrostatic interactions. This may be attributed to the predominance of hydrophobic interactions, which are often not explicitly detected in 2D interaction maps under default visualization parameters. Furthermore, the long alkyl chain of 6-undecylsalicylic acid likely promotes extensive hydrophobic and van der Waals interactions with nonpolar residues within the active pocket, thereby reducing directional interactions such as hydrogen bonding. Despite the absence of specific interaction annotations in the 2D diagram, the 3D visualization demonstrated that 6-undecylsalicylic acid remained well accommodated within the active pocket of COX-2. This observation is supported by its favorable binding energy, suggesting that nonspecific hydrophobic interactions play a major role in stabilizing the ligand–protein complex. Overall, the agreement between the 2D and 3D visualizations indicates that most ligands occupy the same active site as the native ligand, suggesting a potential mechanism of competitive inhibition against the COX-2 enzyme.

3.6. ADMET prediction.

ADMET prediction was performed for Solanapyrone G and 6-undecylsalicylic acid, and the results were compared with those for ibuprofen, a reference compound and a commercially used anti-inflammatory drug. The prediction results are presented in Table 5. Although 6-undecylsalicylic acid exhibited a docking score comparable to that of Solanapyrone G, the latter demonstrated more clearly defined predicted interactions with key COX-2 active-site residues, including ARG120, TYR355, and SER530. In contrast, the predicted binding profile of 6-undecylsalicylic acid appeared to be dominated mainly by hydrophobic interactions within the binding pocket.

In terms of absorption, both 6-undecylsalicylic acid and ibuprofen showed higher predicted intestinal absorption and Caco-2 permeability than Solanapyrone G. Solanapyrone G was also predicted to be a P-glycoprotein substrate, which may reduce its bioavailability

through efflux mechanisms. However, Solanapyrone G demonstrated a more favorable distribution profile, characterized by higher predicted volume of distribution and fraction unbound values. In addition, its low predicted permeability across the blood–brain barrier may indicate limited penetration into the central nervous system. Metabolically, none of the analyzed compounds was predicted to strongly inhibit major cytochrome P450 enzymes, suggesting a relatively low risk of CYP-mediated drug interactions under the computational conditions applied. In terms of excretion, 6-undecylsalicylic acid showed the highest predicted total clearance, followed by Solanapyrone G and ibuprofen, indicating possible differences in elimination rates and pharmacokinetic persistence among the compounds.

Toxicity predictions suggested that Solanapyrone G and 6-undecylsalicylic acid exhibit potentially favorable safety-related characteristics, including negative predictions for AMES mutagenicity, hERG inhibition, hepatotoxicity, and skin sensitization. In contrast, ibuprofen showed positive predictions for hepatotoxicity and skin sensitization in the computational model used in this study. However, ibuprofen is a clinically approved nonsteroidal anti-inflammatory drug (NSAID) with a well-established pharmacological and safety profile supported by extensive clinical evidence. Adverse effects associated with NSAIDs, including hepatotoxicity and hypersensitivity reactions, are generally influenced by dosage, duration of use, and individual patient susceptibility, which computational prediction models may not fully represent. Overall, these findings provide preliminary computational insight into the pharmacokinetic and toxicity-related characteristics of the identified compounds. Nevertheless, all ADMET predictions should be interpreted with caution because they rely solely on computational models and require further experimental validation.

Table 5. Comparison of ADMET (absorption, distribution, metabolism, excretion, and toxicity) profiles of solanapyrone G, 6-undecylsalicylic acid, and ibuprofen based on PKCSM predictions.

Parameter	Solanapyrone G	6-undecylsalicylic acid	Ibuprofen
Absorption			
Water solubility (log mol/L)	-2.152	-2.988	-3.696
Caco-2 permeability (log Papp)	0.339	1.226	1.729
Intestinal absorption (%)	42.6	95.57	94.064
Skin permeability (log Kp)	-2.737	-2.735	-2.685
P-gp substrate	Yes	No	No
P-gp inhibitor	No	No	No
Distribution			
VDss (log L/kg)	0.421	-1.336	-0.803
Fraction unbound (Fu)	0.406	0.142	0.239
BBB permeability (log BB)	-1.407	-0.136	0.31
CNS permeability (log PS)	-3.64	-2.409	-1.695
Metabolism			
CYP2D6 substrate	No	No	No
CYP3A4 substrate	No	No	No
CYP1A2 inhibitor	No	No	No
CYP2C19 inhibitor	No	No	No
CYP2C9 inhibitor	No	No	No
CYP2D6 inhibitor	No	No	No
CYP3A4 inhibitor	No	No	No
Excretion			
Total clearance (log mL/min/kg)	0.587	1.351	0.263
Renal OCT2 substrate	No	No	No
Toxicity			
AMES toxicity	No	No	No
Max tolerated dose (log mg/kg/day)	0.104	0.38	1.015
hERG I inhibitor	No	No	No
hERG II inhibitor	No	No	No
LD50 (mol/kg)	2.328	2.469	2.303
LOAEL (log mg/kg/day)	3.51	2.509	2.438

Parameter	Solanapyrone G	6-undecylsalicylic acid	Ibuprofen
Hepatotoxicity	No	No	Yes
Skin sensitisation	No	No	Yes
T. pyriformis toxicity (log ug/L)	0.286	0.285	0.528
Minnow toxicity (log mM)	4.694	-0.487	0.619

ADMET parameters were predicted using the pkCSM server. Water solubility is expressed as log mol/L; Caco-2 permeability as log Papp (10^{-6} cm/s); intestinal absorption as % absorbed; skin permeability as log Kp; VDss as log L/kg; BBB permeability as log BB; CNS permeability as log PS; total clearance as log mL/min/kg; LD50 as mol/kg; LOAEL as log mg/kg/day; *Tetrahymena pyriformis* toxicity as log µg/L; and minnow toxicity as log mM. CYP = cytochrome P450; P-gp = P-glycoprotein; OCT2 = organic cation transporter 2; hERG = human ether-à-go-go-related gene.

4. Conclusions

This study provides an initial chemical and in silico evaluation of Togaku rheumatic oil as a traditional multiherbal formulation potentially associated with anti-inflammatory activity. LC–MS/MS profiling revealed 13 putatively annotated compounds, reflecting the compositional complexity characteristic of oil-based herbal preparations. Molecular docking analysis suggested that several identified compounds, particularly Solanapyrone G and 6-undecylsalicylic acid, may interact with the COX-2 binding pocket through predicted hydrogen-bonding, hydrophobic, and π-interactions involving key active-site residues such as ARG120, TYR355, and SER530. These findings may provide preliminary insight into potential molecular interactions underlying the traditional use of Togaku rheumatic oil for inflammatory conditions. ADMET prediction further indicated that Solanapyrone G possesses potentially favorable pharmacokinetic and safety-related characteristics under the computational conditions used. However, these findings remain preliminary and should not be interpreted as confirmation of actual biological activity, safety, or therapeutic efficacy. In addition, this study has several limitations, including the use of a single sample, putative LC–MS/MS compound annotation without structural confirmation using authentic standards, the absence of quantitative analytical validation, and the lack of in vitro or in vivo biological evaluation. Therefore, the present work should be considered an initial computational and chemical profiling study that provides preliminary scientific evidence supporting further investigation of Togaku rheumatic oil and its putatively identified constituents. Future studies involving compound isolation, structural confirmation, quantitative analysis, enzyme inhibition assays, and in vivo pharmacological validation are necessary to confirm the biological activity, safety, and mechanisms of action of the identified compounds.

Author Contributions

Conceptualization, E.F., P.M.B., D.A., and R.H.B.S.; methodology, E.F., P.M.B., D.A., and R.H.B.S.; formal analysis, E.F., P.M.B., D.A., and R.H.B.S.; data curation, E.F. and P.M.B.; writing—original draft preparation, E.F., P.M.B., D.A., and R.H.B.S.; writing—review and editing, E.F., P.M.B., D.A., and R.H.B.S. All authors contributed equally to this work and have read and agreed to the published version of the manuscript.

Institutional Review Board Statement

Not applicable.

Informed Consent Statement

Not applicable.

Data Availability Statement

Data supporting the findings of this study are available upon reasonable request from the corresponding author.

Funding

This research received no external funding.

Acknowledgments

The author would like to thank all parties who have contributed to the completion of this research. All authors made equal contributions as the main contributors to this manuscript. No funding resources were reported for this publication.

Conflicts of Interest

The authors declare no conflict of interest.

Role of Funders

The funders had no role in the design of the study, the collection, analysis, or interpretation of data, the writing of the manuscript, or the decision to publish the results.

Abbreviations

The following abbreviations are used in this manuscript:

Abbreviation	Definition
ADMET	Absorption, Distribution, Metabolism, Excretion, and Toxicity
YASARA	Yet Another Scientific Artificial Reality Application
SAVES	Structural Analysis and Verification Server
pkCSM	Pharmacokinetics of Small Molecules
LC-MS/MS	Liquid Chromatography–Tandem Mass Spectrometry

References

1. Zengin, G.; Yagi, S.; Eldahshan, O.A.; Singab, A.N.; Selvi, S.; Rodrigues, M.J.; Custodio, L.; Dall'Acqua, S.; Kumar, M.; Ponnaiya, S.; Aly, S.H. Decoding chemical profiles and biological activities of aerial parts and roots of *Eryngium thorifolium* Boiss by HPLC-MS/MS, GC-MS and *in vitro* chemical assays. *Food Biosci.* **2024**, *61*, 104556, https://doi.org/10.1016/j.fbio.2024.104556.
2. Kumar, K.S.; Sabu, V.; Sindhu, G.; Rauf, A.A.; Helen, A. Isolation, identification and characterization of apigenin from *Justicia gendarussa* and its anti-inflammatory activity. *Int. Immunopharmacol.* **2018**, *59*, 157-167, https://doi.org/10.1016/j.intimp.2018.04.004.
3. Nagulapalli Venkata, K.C.; Swaroop, A.; Bagchi, D.; Bishayee, A. A small plant with big benefits: Fenugreek (Trigonella foenum-graecum Linn.) for disease prevention and health promotion. *Mol. Nutr. Food Res.* **2017**, *61*, 1600950, https://doi.org/10.1002/mnfr.201600950.
4. Aly, S.H.; Uba, A.I.; Nilofar, N.; Majrashi, T.A.; El Hassab, M.A.; Eldehna, W.M.; Zengin, G.; Eldahshan, O.A. Chemical composition and biological activity of lemongrass volatile oil and *n*-Hexane extract: GC/MS analysis, *in vitro* and molecular modelling studies. *PLOS ONE* **2025**, *20*, e0319147, https://doi.org/10.1371/journal.pone.0319147.
5. Peltzer, K.; Pengpid, S. Traditional Health Practitioners in Indonesia: Their Profile, Practice and Treatment

Characteristics. *Complement. Med. Res.* **2018**, *26*, 93-100, https://doi.org/10.1159/000494457.
6. Nurhayati, N.; Widowati, L. The use of traditional health care among Indonesian Family. *Health Sci. J. Indones.* **2017**, *8*, 30-35.
7. Mahendradhata, Y.; Trisnantoro, L.; Listyadewi, S.; Soewondo, P.; Marthias, T.; Harimurti, P.; Prawira, J. The Republic of Indonesia health system review; WHO Regional Office for South-East Asia: **2017**; Volume 7.
8. Beis, O.; Seran, L.; Nau, G. Studi etnofarmakognosi tumbuhan berkhasiat obat untuk mengobati penyakit pada manusia di Desa Teas Kecamatan Noebeba Kabupaten Timor Tengah Selatan. *J. Gatranusantara* **2022**, *20*, 46-57.
9. Huki, A.Y.P.; Seran, L.; Buku, M.N.I. Jenis – jenis tumbuhan yang digunakan untuk mengobati penyakit pada manusia oleh masyarakat desa Nunusunu Kecamatan Kualin Kabupaten Timor Tengah Selatan. *JBIOEDRA: Jurnal Pendidikan Biologi* **2023**, *1*, 141-150.
10. Belem, K.; e, W.L.M.E.; Kabor; e, B.; Compaor; e-Coulibaly, A.; Traor; e, T.K.; Thiombiano, E.A.M.; Nebi; e, T.; e, M.; Compaor; e, M.; Kini, F.; elix, B.; Ou; edraogo, S.; Kiendrebeogo, M. Phytochemical and biological investigations of extracts from the roots of Cocos nucifera L.(Arecaceae) and Carica papaya L.(Caricaceae), two plants used in traditional medicine. *Afr. J. Biochem. Res.* **2021**, *15*, 28-35, https://doi.org/10.5897/AJBR2020.1107.
11. Sharma, L.D.; Khan, M.R.; Devi, A.K. Methanolic and ethanolic phytochemical screening of Sweet flag (Acorus calamus L.) rhizome. *J. Drug Deliv. Ther.* **2023**, *13*, 114-118, https://doi.org/10.22270/jddt.v13i9.6223.
12. Mao, Q.-Q.; Xu, X.-Y.; Cao, S.-Y.; Gan, R.-Y.; Corke, H.; Beta, T.; Li, H.-B. Bioactive Compounds and Bioactivities of Ginger (*Zingiber officinale* Roscoe). *Foods* **2019**, *8*, 185, https://doi.org/10.3390/foods8060185.
13. Yang, B.-Y.; Luo, Y.-M.; Liu, Y.; Yin, X.; Zhou, Y.-Y.; Kuang, H.-X. New lignans from the roots of *Datura metel* L. *Phytochem. Lett.* **2018**, *28*, 8-12, https://doi.org/10.1016/j.phytol.2018.08.002.
14. Made Ratih, G.A.; Imawati, M.F.; Nugroho, R.R.; Purwanti, D.I.; Wongso, S.; Prajogo, B.; Indrayanto, G. Phytochemicals of Gandarusa (Justicia gendarussa) and Its Preparations. *Nat. Prod. Commun.* **2019**, *14*, 1934578X19851406, https://doi.org/10.1177/1934578X19851406.
15. Jain, T.; Singh, M.P.; Bhardwaj, H.; Gohil, K.J. Review on pharmacology activities of *Justicia Gendarussa Burm* F. *Pharmacol. Res. - Mod. Chin. Med.* **2024**, *10*, 100339, https://doi.org/10.1016/j.prmcm.2023.100339.
16. Šnirc, M.; Lidiková, J.; Čeryová, N.; Pintér, E.; Ivanišová, E.; Musilová, J.; Vollmannová, A.; Rybnikár, S. Mineral and phytochemical profiles of selected garlic (*Allium sativum* L.) cultivars. *S. Afr. J. Bot.* **2023**, *158*, 319-325, https://doi.org/10.1016/j.sajb.2023.05.024.
17. González-de-Peredo, A.V.; Vázquez-Espinosa, M.; Espada-Bellido, E.; Ferreiro-González, M.; Carrera, C.; Barbero, G.F.; Palma, M. Extraction of Antioxidant Compounds from Onion Bulb (*Allium cepa* L.) Using Individual and Simultaneous Microwave-Assisted Extraction Methods. *Antioxidants* **2022**, *11*, 846, https://doi.org/10.3390/antiox11050846.
18. Taguimjeu, P.L.K.T.; Tchatat Tali, M.B.; Dongmo, K.J.J.; Fongang, Y.S.F.; Fauconnier, M.-L.; Lenta, B.N.; Boyom, F.F.; Sewald, N.; Ngouela, S.A. Chemical constituents of the leaves and roots of *Lantana camara* Linn (Verbenaceae) display good *in vitro* antiplasmodial potency and ADMET properties. *S. Afr. J. Bot.* **2025**, *185*, 66-79, https://doi.org/10.1016/j.sajb.2025.07.039.
19. Basera, P.; Lavania, M.; Agnihotri, A.; Lal, B. Analytical Investigation of *Cymbopogon citratus* and Exploiting the Potential of Developed Silver Nanoparticle Against the Dominating Species of Pathogenic Bacteria. *Front. Microbiol.* **2019**, *10*, 282, https://doi.org/10.3389/fmicb.2019.00282.
20. Chandan, G.; Kumar, C.; Chibber, P.; Kumar, A.; Singh, G.; Satti, N.K.; Gulilat, H.; Saini, A.K.; Bishayee, A.; Saini, R.V. Evaluation of analgesic and anti-inflammatory activities and molecular docking analysis of steroidal lactones from *Datura stramonium* L. *Phytomedicine* **2021**, *89*, 153621, https://doi.org/10.1016/j.phymed.2021.153621.
21. Ullah, R.; Badshah, W.; Ali, G.; Ullah, A.; Khan, S.U.; Ahmad, N.; Shahid, M.; Naveed, M.; Ullah, S.; Bangash, S.A.; Althobaiti, Y.S. *Cassia artemisiodes* attenuates nociceptive and diabetes-induced neuropathic pain modalities apropos antioxidant and anti-inflammatory mechanisms. *Biomed. Pharmacother.* **2022**, *149*, 112834, https://doi.org/10.1016/j.biopha.2022.112834.
22. Muniandy, K.; Gothai, S.; Badran, K.M.H.; Suresh Kumar, S.; Esa, N.M.; Arulselvan, P. Suppression of Proinflammatory Cytokines and Mediators in LPS-Induced RAW 264.7 Macrophages by Stem Extract of

Alternanthera sessilis via the Inhibition of the NF-κB Pathway. *J. Immunol. Res.* **2018**, *2018*, 3430684, https://doi.org/10.1155/2018/3430684.

23. Akanda, M.R.; Kim, I.-S.; Ahn, D.; Tae, H.-J.; Nam, H.-H.; Choo, B.-K.; Kim, K.; Park, B.-Y. Anti-Inflammatory and Gastroprotective Roles of *Rabdosia inflexa* through Downregulation of Pro-Inflammatory Cytokines and MAPK/NF-κB Signaling Pathways. *Int. J. Mol. Sci.* **2018**, *19*, 584, https://doi.org/10.3390/ijms19020584.
24. Friardi, I.; Widi Novella, D.; Nurwahidatul, A.; Rustini, R.; Deddi Prima, P. TLC-Bioautographic and LC-MS/MS Detection of Antimicrobial Compounds from Four Semipolar Extracts of Cladonia Species. In Proceedings of the Proceedings of the 2nd International Conference on Contemporary Science and Clinical Pharmacy 2021 (ICCSCP 2021), Online, 9-10 September 2021; Atlantis Press: **2021**; pp. 49-59, https://doi.org/10.2991/ahsr.k.211105.008.
25. Blaženović, I.; Kind, T.; Sa, M.R.; Ji, J.; Vaniya, A.; Wancewicz, B.; Roberts, B.S.; Torbašinović, H.; Lee, T.; Mehta, S.S.; Showalter, M.R.; Song, H.; Kwok, J.; Jahn, D.; Kim, J.; Fiehn, O. Structure Annotation of All Mass Spectra in Untargeted Metabolomics. *Anal. Chem.* **2019**, *91*, 2155-2162, https://doi.org/10.1021/acs.analchem.8b04698.
26. Ifora, I.; Putri, A.; Oktavia, S. Vitex trifolia as Cyclooxygenase-2 Inhibitors in Anti-Inflammatory Drug Discovery. *Int. J. Pharm. Bio Med. Sci.* **2022**, *2*, 400-406, https://doi.org/10.47191/ijpbms/v2-i10-03.
27. Orlando, B.J.; Malkowski, M.G. Crystal structure of rofecoxib bound to human cyclooxygenase-2. *Acta Cryst.* **2016**, *F72*, 772-776, https://doi.org/10.1107/S2053230X16014230.
28. Colovos, C.; Yeates, T.O. Verification of protein structures: Patterns of nonbonded atomic interactions. *Protein Sci.* **1993**, *2*, 1511-1519, https://doi.org/10.1002/pro.5560020916.
29. Laskowski, R.A.; MacArthur, M.W.; Moss, D.S.; Thornton, J.M. PROCHECK: a program to check the stereochemical quality of protein structures. *J. Appl. Cryst.* **1993**, *26*, 283-291, https://doi.org/10.1107/S0021889892009944.
30. Pontius, J.; Richelle, J.; Wodak, S.J. Deviations from Standard Atomic Volumes as a Quality Measure for Protein Crystal Structures. *J. Mol. Biol.* **1996**, *264*, 121-136, https://doi.org/10.1006/jmbi.1996.0628.
31. Bowie, J.U.; Lüthy, R.; Eisenberg, D. A Method to Identify Protein Sequences That Fold into a Known Three-Dimensional Structure. *Science* **1991**, *253*, 164-170, https://doi.org/10.1126/science.1853201.
32. Wiederstein, M.; Sippl, M.J. ProSA-web: interactive web service for the recognition of errors in three-dimensional structures of proteins. *Nucleic Acids Res.* **2007**, *35*, W407-W410, https://doi.org/10.1093/nar/gkm290.
33. Xu, Y.; Wang, S.; Hu, Q.; Gao, S.; Ma, X.; Zhang, W.; Shen, Y.; Chen, F.; Lai, L.; Pei, J. CavityPlus: a web server for protein cavity detection with pharmacophore modelling, allosteric site identification and covalent ligand binding ability prediction. *Nucleic Acids Res.* **2018**, *46*, W374-W379, https://doi.org/10.1093/nar/gky380.
34. Gholam, G.M.; Irsal, R.A.P.; Mahendra, F.R.; Dwicesaria, M.A.; Siregar, J.E.; Ansori, A.N.M.; Zainul, R. In silico computational prediction of *Saussurea pulchella* compounds with inhibitory effects on plasmepsin X in *Plasmodium falciparum*. *Inform. Med. Unlocked* **2024**, *49*, 101549, https://doi.org/10.1016/j.imu.2024.101549.
35. Safithri, M.; Koendhori, E.B.; Andrianto, D.; Kurniasih, R.; Dwicesaria, M.A.; Nurinsani, E.Y.Y.; Umar, M.A.; Hudayanti, M. Analysis of Bioactive Compounds Piper crocatum as Inhibitors of Acetylcholinesterase In Silico and In Vitro. *Trends Sci.* **2025**, *22*, 9437, https://doi.org/10.48048/tis.2025.9437.
36. Pires, D.E.V.; Blundell, T.L.; Ascher, D.B. pkCSM: Predicting Small-Molecule Pharmacokinetic and Toxicity Properties Using Graph-Based Signatures. *J. Med. Chem.* **2015**, *58*, 4066-4072, https://doi.org/10.1021/acs.jmedchem.5b00104.
37. Schymanski, E.L.; Jeon, J.; Gulde, R.; Fenner, K.; Ruff, M.; Singer, H.P.; Hollender, J. Identifying Small Molecules via High Resolution Mass Spectrometry: Communicating Confidence. *Environ. Sci. Technol.* **2014**, *48*, 2097-2098, https://doi.org/10.1021/es5002105.
38. Kim, Y.-T.; Shin, J.-S.; Ye, S.-J.; Kim, J.H.; Eom, S.H.; Baik, M.-Y. Conversion of gingerols to shogaols in ginger (*Zingiber officinale roscoe*) by puffing. *Food Chemistry* **2024**, *452*, 139425, https://doi.org/10.1016/j.foodchem.2024.139425.
39. Tavares, L.; Santos, L.; Zapata Noreña, C.P. Bioactive compounds of garlic: A comprehensive review of encapsulation technologies, characterization of the encapsulated garlic compounds and their industrial applicability. *Trends Food Sci. Technol.* **2021**, *114*, 232-244, https://doi.org/10.1016/j.tifs.2021.05.019.

40. Williams, M.L.; Olomukoro, A.A.; Emmons, R.V.; Godage, N.H.; Gionfriddo, E. Matrix effects demystified: Strategies for resolving challenges in analytical separations of complex samples. *J. Sep. Sci.* **2023**, *46*, 2300571, https://doi.org/10.1002/jssc.202300571.
41. Jiahua, C.; Jinping, J. Natural COX-2 Inhibitors as Promising Anti-inflammatory Agents: An Update. *Curr. Med. Chem.* **2021**, *28*, 3622-3646, https://doi.org/10.2174/0929867327999200917150939.
42. Hengphasatporn, K.; Harada, R.; Wilasluck, P.; Deetanya, P.; Sukandar, E.R.; Chavasiri, W.; Suroengrit, A.; Boonyasuppayakorn, S.; Rungrotmongkol, T.; Wangkanont, K.; Shigeta, Y. Promising SARS-CoV-2 main protease inhibitor ligand-binding modes evaluated using LB-PaCS-MD/FMO. *Sci. Rep.* **2022**, *12*, 17984, https://doi.org/10.1038/s41598-022-22703-1.
43. Sun, Q.; Wang, H.; Xie, J.; Wang, L.; Mu, J.; Li, J.; Ren, Y.; Lai, L. Computer-Aided Drug Discovery for Undruggable Targets. *Chem. Rev.* **2025**, *125*, 6309-6365, https://doi.org/10.1021/acs.chemrev.4c00969.
44. Timofeevski, S.L.; Prusakiewicz, J.J.; Rouzer, C.A.; Marnett, L.J. Isoform-Selective Interaction of Cyclooxygenase-2 with Indomethacin Amides Studied by Real-Time Fluorescence, Inhibition Kinetics, and Site-Directed Mutagenesis. *Biochemistry* **2002**, *41*, 9654-9662, https://doi.org/10.1021/bi0203637.
45. Chaudhary, N.; Aparoy, P. Deciphering the mechanism behind the varied binding activities of COXIBs through Molecular Dynamic Simulations, MM-PBSA binding energy calculations and per-residue energy decomposition studies. *J. Biomol. Struct. Dyn.* **2017**, *35*, 868-882, https://doi.org/10.1080/07391102.2016.1165736.
46. Desiraju, G.R.; Gopalakrishnan, B.; Jetti, R.K.R.; Nagaraju, A.; Raveendra, D.; Sarma, J.A.R.P.; Sobhia, M.E.; Thilagavathi, R. Computer-Aided Design of Selective COX-2 Inhibitors: Comparative Molecular Field Analysis, Comparative Molecular Similarity Indices Analysis, and Docking Studies of Some 1,2-Diarylimidazole Derivatives. *J. Med. Chem.* **2002**, *45*, 4847-4857, https://doi.org/10.1021/jm020198t.
47. Carbone, J.; Ghidini, A.; Romano, A.; Gentilucci, L.; Musiani, F. PacDOCK: A Web Server for Positional Distance-Based and Interaction-Based Analysis of Docking Results. *Molecules* **2022**, *27*, 6884, https://doi.org/10.3390/molecules27206884.
48. Guterres, H.; Im, W. CHARMM-GUI-Based Induced Fit Docking Workflow to Generate Reliable Protein–Ligand Binding Modes. *J. Chem. Inf. Model.* **2023**, *63*, 4772-4779, https://doi.org/10.1021/acs.jcim.3c00416.
49. Heras Martínez, H.M.; Sánchez-Ramírez, B.; Landeros-Martínez, L.-L.; Rodríguez-Guerrero, D.; Espinoza-Hicks, J.C.; Zaragoza-Galán, G.; Bugarin, A.; Chávez-Flores, D. Phthalimide Derivatives as Anti-Inflammatory Agents: In Silico COX-2 Targeting and In Vitro Inhibition of PGE_2 Production. *Pharmaceutics* **2026**, *18*, 129, https://doi.org/10.3390/pharmaceutics18010129.
50. Oniga, S.D.; Pacureanu, L.; Stoica, C.I.; Palage, M.D.; Crăciun, A.; Rusu, L.R.; Crisan, E.-L.; Araniciu, C. COX Inhibition Profile and Molecular Docking Studies of Some 2-(Trimethoxyphenyl)-Thiazoles. *Molecules* **2017**, *22*, 1507, https://doi.org/10.3390/molecules22091507.

Publisher's Note & Disclaimer